Articles

Evolution of Microstructure during the Thermal Activation of Chromium-Promoted Tin(IV) Oxide Catalysts: An FT-IR, FT-Raman, XRD, TEM, and XANES/EXAFS Study

Philip G. Harrison,* Nicholas C. Lloyd, Wayne Daniell, Craig Bailey, and Wan Azelee[†]

School of Chemistry, University of Nottingham, University Park, Nottingham NG7 2RD, U.K.

Received May 13, 1998. Revised Manuscript Received October 26, 1998

The chemical transformations occurring during the thermal activation of chromium-promoted tin(IV) oxide catalysts have been investigated by vibrational spectroscopy (FT-IR and FT-Raman), powder X-ray diffraction, transmission electron microscopy, and extended X-ray absorption fine structure and near-edge structure. Three methods of catalyst preparation have been employed: impregnation of SnO_2 using aqueous CrO_3 solutions, impregnation of SnO_2 using aqueous chromium(III) nitrate solutions, and coprecipitation from aqueous solutions containing both tin(IV) and chromium(III) ions. The freshly prepared gel catalyst materials comprise small (ca. 1−2 nm) particles of hydrous tin(IV) oxide, on the surface of which are sorbed chromate(VI) anions, $\{Cr(H_2O)_6^{3+}\}$ cations, or polymeric γ-CrOOH depending on the preparative route. In all three cases, however, calcination at 573 K results in the formation of the mixed-valence chromium compound Cr_5O_{12}. At higher calcination temperatures Cr_2O_3 is formed, which becomes more crystalline the higher the temperature. Concurrently, the size of the tin(IV) oxide particles increases, only slowly initially (ca. ×2 by 673 K and ca. ×4 by 873 K), but sintering to very large particles occurs at higher temperatures. No incorporation of chromium into the tin(IV) oxide lattice occurs even at high temperature.

Introduction

The control of noxious emissions resulting either from the combustion of fossil fuels or from other industrial activities is one of the most immediate and compelling problems faced by nearly every country in the world. The levels of pollutants from automobiles, carbon monoxide (CO), hydrocarbons (HCs), and nitrogen oxides (NO_x), are the subject of ever increasingly stringent legislation controlling the maximum permitted levels of emissions of each substance. Platinum group catalysts currently represent the state-of-the-art in internal combustion engine emission technology. The driving force for the development of non-platinum exhaust emission catalysts is the price, strategic importance, and low availability of the platinum group metals. Tin oxide based materials have been known for a long time to have good activity toward the CO/O_2 and CO/NO reactions.[1−7] Data from our laboratory[8] have demonstrated that Cr/SnO_2 and $Cu/Cr/SnO_2$ catalysts exhibit three-way activity which is comparable to conventional noble metal catalysts. These data show that the performance of these catalysts is similar to that of the $Pt/Rh/Al_2O_3$ catalyst for CO and HC oxidation.

Despite this very promising observed activity, however, the constitution of these catalyst materials is essentially unknown. Even simple questions such as the oxidation state of chromium in the active catalyst remain unanswered. Information on mixed tin(IV) oxide materials is sparse. Simple surface area data have been reported for SnO_2/PdO,[9] SnO_2/V_2O_5, SnO_2/P_2O_5, SnO_2/MoO_3,[10] and SnO_2/MO (M = Co, Mn, Fe, Cr, Ni, Cu).[11] We have reported the preparation of $Cr(VI)/SnO_2$ catalyst materials by impregnation of tin(IV) oxide using

[†] Present address: Department of Chemistry, Faculty of Science, University Technology Malaysia, Skudai, Locked Beg 791, 80990 Johor Bahru, Malaysia.

(1) Fuller, M. J.; Warwick, M. E. *J. Catal.* **1973**, *29*, 441.
(2) Fuller, M. J.; Warwick, M. E. *J. Catal.* **1974**, *34*, 445.
(3) Bond, G. C.; Molloy, L. R.; Fuller, M. J. *J. Chem. Soc., Chem. Commun.* **1975**, 796.
(4) Croft, G.; Fuller, M. J. *Nature* **1977**, *269*, 585.
(5) Fuller, M. J.; Warwick, M. E. *J. Catal.* **1976**, *42*, 418.
(6) Fuller, M. J.; Warwick, M. E. *Chem. Ind. (London)* **1976**, 787.
(7) Solymosi, F.; Kiss, J. *J. Catal.* **1978**, *54*, 42.
(8) Harrison, P. G.; Harris, P. J. U.S. Patent 4 908 192, 1990; U.S. Patent 5 051 393, 1991.
(9) Croft, G.; Fuller, M. J. *Nature* **1977**, *269*, 585.
(10) Ai, M. *J. Catal.* **1975**, *40*, 318, 327.
(11) Fuller, M. J.; Warwick, M. E.; Walton, A. *J. Appl. Chem. Biotechnol.* **1978**, *28*, 539.

10.1021/cm980347p CCC: $18.00
Published on Web 03/31/1999

aqueous CrO_3 solutions,[8] while Solymosi[12] has reported a SnO_2/Cr_2O_3 catalyst prepared by adding Cr_2O_3 to a suspension of SnO_2 and stirring until the material was homogeneous. The resultant catalyst material was described as containing higher valence chromium ions stabilized in the surface layer of SnO_2 although no charactization data were reported.

To overcome the obvious lack of information in this area, here we report data describing Cr/SnO_2 catalyst materials prepared via three routes: impregnation of SnO_2 using aqueous CrO_3 solutions, impregnation of SnO_2 using aqueous chromium(III) nitrate solutions, and coprecipitation from aqueous solutions containing both tin(IV) and chromium(III) ions. Coprecipitation is not available for the preparation of $Cr(VI)/SnO_2$ catalyst materials because no chromium(VI) is incorporated into the precipitated solids. A priori, it might be expected that coprecipitation from solutions containing more than one metal cation would give rise to an oxide material in which the two cations are uniformly dispersed within the freshly precipitated oxide particles. In contrast, the impregnation route would locate modifying or promoting metal ions on the surface of the primary particles of the metal oxide support, in the present case tin(IV) oxide. Optimum catalytic activity in catalyst materials such as these is produced via thermal preactivation processing, usually in the temperature range 573−673 K, although heating to much higher temperatures invariably results in a significant lowering of activity. Many different changes, both chemical and physical, can occur during such thermal processing including sintering, change in pore texture, migration of hetero ions, phase separation, etc. It is, therefore, of critical importance for the understanding of the operation of this type of catalyst system to gain a knowledge of their fundamental constitution and behavior on thermal treatment. Catalysts comprising chromium supported on several other metal oxides have been studied extensively;[13] however, little is known concerning the Cr/SnO_2 system. Hence, in this paper we describe the nature of as-prepared Cr/SnO_2 catalyst materials as well as after calcination processing using a number of techniques including vibrational spectroscopy (FT-IR and FT-Raman), powder X-ray diffraction (XRD), transmission electron microscopy (TEM), and extended X-ray absorption fine structure and near-edge structure (XANES/EXAFS).

It should be noted, however, that although the catalytic activity of these materials is comparable and, in some circumstances, superior to platinum group metal catalysts, a major concern is the presence of chromium as a promoter. The toxicity, mutagenic effects, and carcinogenicity of chromium compounds are well documented, and the adverse health effects suffered by workers exposed to Cr(VI) have also been studied extensively.[14−17] Such factors would most probably have an adverse effect on the commercialization of this particular type of catalyst for automobile purposes. Nevertheless, these data shed important light in the area of transition-metal-promoted tin(IV) oxide oxidation catalyst materials.

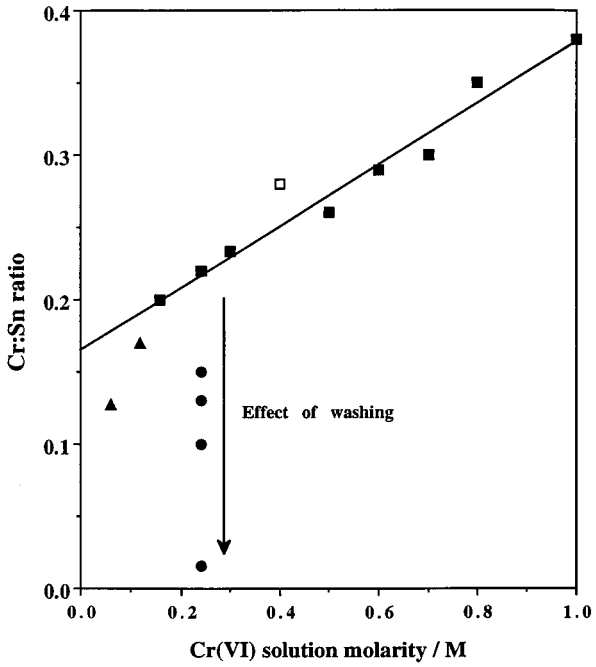

Figure 1. Plot of the final Cr:Sn atom ratio in the $Cr(VI)/SnO_2$ catalyst versus molarity of the aqueous CrO_3 solution. See the text for an explanation of symbols and conditions. The straight line represents the best least-squares fit to the linear portion of the plot ({Cr:Sn} = 0.164 + 0.213[Cr(VI)], R^2 = 0.979).

Experimental Section

Preparation of Catalyst Materials. *(a) Tin(IV) Oxide Gel.* Tin(IV) oxide gel was precipitated by the dropwise addition of concentrated 33% w/w AnalaR aqueous ammonia solution to a cold, vigorously stirred solution of 0.1 M (13 g, 33.69 mL by volume) tin(IV) chloride (Aldrich) in triply distilled water (ca. 500 mL) to a final pH of 4, to give an average particle size of 2.0 nm (TEM). The gelatinous precipitate formed was washed free of chloride ion by repeated centrifuging and redispersing in triply distilled water. This was confirmed by a simple negative chloride ion test using a silver nitrate solution. The solid, white gel obtained was then allowed to air-dry at 333 K for 2−3 days. At this stage the gel was of a granular appearance and approximately one-tenth of its initial volume. These large granules were then broken down by pouring a small amount of triply distilled water over them and then were allowed to air-dry further at 333 K for 24 h. The dry, colorless gel was then ground into a fine white powder.

(b) Chromium(VI)-Promoted Tin(IV) Oxide. To a suspension of tin(IV) oxide (10 g) was added chromic acid (160 mL), a solution of chromium(VI) oxide (CrO_3, Aldrich) dissolved in triply distilled water. The mixture was stirred for 18 h under gentle reflux conditions, after which the resultant yellowish suspension was filtered to yield a yellow powder which was dried in air at 333 K for 24 h. The Cr:Sn atomic ratio in the catalyst could be controlled by modifying the initial solution concentration of the chromium(VI) oxide solution. Figure 1 shows the linear relationship, using the conditions described above, between the initial solution concentration and the Cr:Sn ratio in the $Cr(VI)/SnO_2$ gel over the solution concentration range of 0.05−1.0 M after the materials had been dried in air at ambient temperature (Figure 1, points marked ▲ and ■). In the concentration range 0.2−1.0 M there is a linear relationship between the final Cr:Sn ratio and the concentra-

(12) Solymosi, F.; Kiss, J. *J. Chem. Soc., Chem. Commun.* **1974**, 509.
(13) Weckhuysen, B. M.; Wachs, I. E.; Schoonheydt, R. A. *Chem. Rev.* **1996**, *96*, 3327.
(14) Langard, S.; Norseth, T. In *Handbook on the Toxicology of Metals*; Friberg, L., Nordberg, G. F., Vouk, V., Eds.; Elsevier: Amsterdam, The Netherlands, 1986; Chapter 8.
(15) Hayes, R. B. *Sci. Total Environ.* **1988**, *71*, 331.
(16) Sanz, R. *J. Occup. Med.* **1989**, *31*, 1013.
(17) Cieslak-Golonka, M. *Polyhedron* **1995**, *15*, 3667.

Table 1. Loading Data for Cr(III)/SnO_2-cop Catalyst Materials

catalyst stoichiometry[a]	
target	resultant[b]
10Cr:90Sn	10Cr:90Sn (Cr:Sn 0.11)
20Cr:80Sn	9.5Cr:90.5Sn (Cr:Sn 0.105)
30Cr:70Sn	24Cr:76Sn (Cr:Sn 0.32)

[a] Atom percent. [b] Atom/atom ratio in parentheses.

Table 2. Color Changes Observed on Calcination of Chromium-Promoted Tin(IV) Oxide Catalyst Materials

	calcination temperature/K			
catalyst sample	333	573	873	1273
Cr(VI)/SnO_2-imp	yellow	light brown	red/brown	dark green
Cr(III)/SnO_2-imp	light green	yellow	maroon	grey
Cr(III)/SnO_2-cop	dark green	light brown/ black	red/brown	green

tion of the Cr(VI) solution (see caption for Figure 1), but at concentrations lower than 0.1 M less chromium(VI) is adsorbed than is expected from this relationship. Targeting a specific loading was reproducible under the same preparative conditions, although varying the conditions changed the loading. For example, increasing the time of exposure to the chromium(VI) oxide solution to 24 h resulted in an increased Cr:Sn ratio (Figure 1, point marked □). However, washing the impregnated materials with triply distilled water during the filtration stage results in a marked decrease in the overall loadings. For example, washing the Cr(VI)/SnO_2 (Cr:Sn 0.22) catalyst material reduces the Cr:Sn ratio progressively to 0.016 after washing with aliquots of water totalling 135 mL (Figure 1, points marked ●). Therefore, it can be concluded that targeting a specific loading for chromium(VI) depends on various criteria including the initial chromium(VI) solution concentration, exposure time, reflux temperature, and washing conditions. Samples prepared by this route are referred to as Cr(VI)/SnO_2-imp with the Cr:Sn atom ratio denoted in parentheses.

(c) Chromium(III)-Promoted Tin(IV) Oxide by Impregnation. To a suspension of tin(IV) oxide gel (10 g) was added an aqueous solution of $Cr(NO_3)_3 \cdot 9H_2O$ (Aldrich) dissolved in triply distilled water. These mixtures were kept stirred for 18 h, and the resultant suspension was filtered to yield a pale green gel, which was was then air-dried at 333 K for 24 h. The Cr:Sn atomic ratio in the catalyst could be controlled by modifying the initial solution concentration of the chromium(III) nitrate solution, and as with chromium(VI) targeting a specific loading was reproducible under the same preparative conditions. This material is referred to as Cr(III)/SnO_2-imp with the Cr:Sn atom ratio denoted in parentheses.

(d) Chromium(III)-Promoted Tin(IV) Oxide by Coprecipitation. This was achieved by a modification of the precipitation method above. $Cr(NO_3)_3 \cdot 9H_2O$ was allowed to dissolve and homogenize in the vigorously stirred solution of tin(IV) chloride prior to addition of base. The subsequent workup was as above, affording a dark green gel. The Cr:Sn atom ratio was varied by varying the Cr:Sn ratio in the initial aqueous solution prior to addition of base. Materials prepared by this route are referred to as Cr(III)/SnO_2-cop with the Cr:Sn atom ratio denoted in parentheses. Cr:Sn atom ratios for these materials are tabulated in Table 1.

Catalyst Thermal Pretreatment. Catalyst materials (approximately 2 g aliquots) were calcined in an alumina boat for 24 h using a Vecstar 91e tube furnace at temperatures of 573, 673, 873, 1073, and 1273 K. Many color changes were observed for each sample type (Table 2) indicating various transformations in dopant oxidation state and phase.

Physical and Spectroscopic Measurements. Catalyst stoichiometries were determined by atomic absorption (for Cr(III)/SnO_2-imp and Cr(VI)/SnO_2-imp materials) and X-ray fluorescence (Philips PW1480 wavelength dispersive instrument) (for Cr(III)/SnO_2-cop materials).

Powder X-ray diffraction data were acquired using a Philips X-pert system fitted with a PW 1710 diffractometer control unit with Cu Kα radiation (λ = 1.5405 Å). Representative diffractograms were acquired over 5−80° 2θ with 0.02° steps and 0.4 s acquisition times/step. DICVOL91[18] was used for indexing. Data for Rietveld refinement[19] were acquired over values of 5−120° 2θ with 0.02° steps and 9.5 s acquisition times/step.

Infrared spectra were obtained from KBr disk samples using a Nicolet 20SXC spectrometer. A total of 32 scans were recorded for each sample at a resolution of 1 cm^{-1}. FT-Raman spectra were obtained as neat powders using a Perkin-Elmer 2000 NIR FT-Raman spectrometer equipped with a Nd^{3+}-YAG laser operating at a power of 50−200 mW. Samples were packed in a small capillary tube approximately 1 cm in length, and 160 scans/sample were recorded at a resolution of 4 cm^{-1}. No sample damage was apparent.

EXAFS measurements were performed on station 8.1 at the Daresbury Laboratory, Warrington, U.K., which operates at an energy of up to 2.0 GeV and a maximum beam current of 200 mA. The X-rays are vertically collimated, producing a beam of less than 1 mrad divergence. A Si(111) double-crystal monochromator was used to select a single wavelength beam of X-rays, the tuneable energy range that can be achieved using this monochromator is 2−10 keV. A total of 40−50% of the X-ray beam was rejected to filter out the undesired harmonics while retaining 50−60% of the primary beam intensity.

Data were collected at the Cr K-edge (8.978 keV) in fluorescence mode utilizing a Ge-13 channel solid-state detector. The sample was positioned at ca. 45° to the incident to maximize the solid angle seen by the detector. Six scans were recorded for each catalyst sample, and refinement was achieved using EXBACK, EXCALIB, and EXCURV92.[20] The scans were co-aligned, spikes due to noise removed, and the total number of scans added together to produce a single output data set with an improved signal-to-noise using EXCALIB. Background X-ray absorption was removed from the summed data set in two stages using the program EXBACK. Initially the preedge background was determined by fitting this region to a polynomial usually of order 1. The background absorption was then removed from the postedge region by a series of linked polynomial curves (normally 2 or 3) of order 3. With both the preedge and postedge background absorption removed from the data, the x axis was converted from energy to k space ($k = 2\pi/\lambda$, where λ is the electron wavelength) to give the EXAFS oscillations form k = 0. The EXAFS oscillations were then multiplied to k^3 to increase the amplitude of the oscillations at high values of k. Finally, radial distribution spectra were obtained via Fourier transformation of the EXAFS data. EXCURV92 was used to simulate EXAFS spectra of radial shells of neighbors around the central atom. For a more detailed description of the curved wave theory used in the program to calculate theoretical backscattering amplitudes and phase shifts, the reader is directed to the publications of Gurman[21] and Lee.[22]

The fit correlation parameter R between the calculated and observed data for the Cr(III)/SnO_2-imp and Cr(III)/SnO_2-cop fall in the very acceptable range 20−40. Values of $R < 50$ are very reasonable for this type of sample, and values of $R < 20$ are unobtainable except for crystalline structures of clearly defined geometries. Values of R for Cr(VI)/SnO_2-imp are somewhat higher in the range 50−60 but nevertheless are still acceptable.

The estimated levels of accuracy in the refinements made by the EXCURV92 program arising from imperfect transferability of phase shifts and the fitting procedures are coordination number (50%), Debye−Waller factor 2σ^2 (50%), and radii (0.02 Å).

(18) DICVOL91: Boultif, A.; Louer, D. *J. Appl. Crystallogr.* **1991**, *24*, 987.
(19) PC−Rietveld Plus, Philips, June 1993.
(20) EXBACK, EXCALIB, and EXCURV92, Daresbury Computer programs, Daresbury Laboratory, Cheshire, U.K.
(21) Gurman, S. J.; Binstedt, N.; Ross, I. *J. Phys. C* **1984**, *17*, 143; **1986**, *19*, 1845.
(22) Lee, P. A.; Pendry, J. B. *Phys. Rev. B* **1975**, *11*, 2795.21.

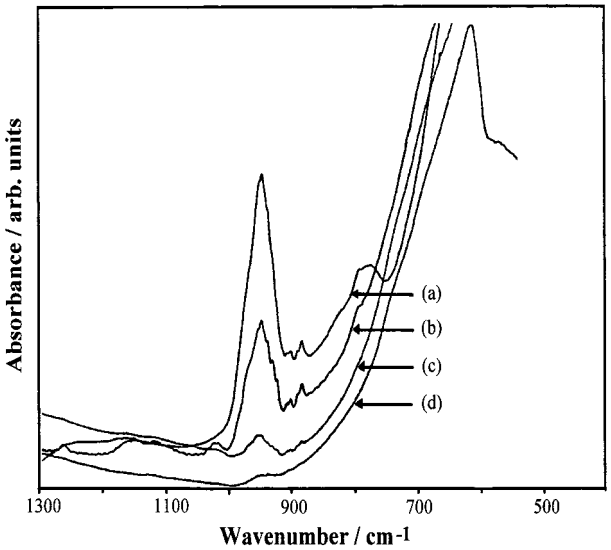

Figure 2. Mid-infrared spectra of Cr(VI)/SnO_2-imp (Cr:Sn 0.38) after thermal treatment at (a) 333, (b) 573, (c) 873, and (d) 1273 K.

TEM were recorded using a JEOL 2000FX transmission electron microscope at the Department of Materials Engineering and Materials Design, University of Nottingham, operating at an accelerating voltage of 200 kV. Catalyst samples were sonicated in dry chloroform for 15 min, and 1 drop of the resultant suspension was then allowed to dry upon a holey carbon-coated copper TEM grid.

Results

Mid-FT-IR Spectroscopy Studies. Freshly prepared tin(IV) oxide based gels exhibit an intense, very broad hydroxyl stretching envelope due to adsorbed molecular water ranging from ca. 3600 to 2500 cm^{-1} with a maximum at ca. 3437 cm^{-1}, which shifts to higher wavenumber on increasing calcination temperature. The corresponding water deformation mode is centered at ca. 1640 cm^{-1}. Increasing the calcination temperature results in a decrease in the intensity of the molecular water band. That this band is still observable even after calcination at 1273 K is most probably because the spectra were not recorded in situ and some readsorption of molecular water from the ambient atmosphere has occurred. The intense broad band observed at ca. 610 cm^{-1} (Figure 2) for freshly prepared Cr(VI)/SnO_2-imp (Cr:Sn 0.38) increases in intensity and sharpens as the temperature of the heat treatment is increased. This band is assigned to the antisymmetric Sn−O−Sn stretching modes of the surface-bridging oxide formed by condensation of adjacent surface hydroxyl groups. Corroboration of this is gained from the evolution and subsequent loss of surface hydroxyl deformation bands. Calcination at 573 K produces clearly resolved bands at ca. 1260 and 1150 cm^{-1} which are lost after the material has been calcined at temperatures of ≥873 K, similar to the behavior previously observed for tin(IV) oxide gel itself.[23] After calcination at 1273 K, the Sn−O−Sn band reaches a maximum at ca. 620 cm^{-1} compared with ν_{as}(SnOSn) of

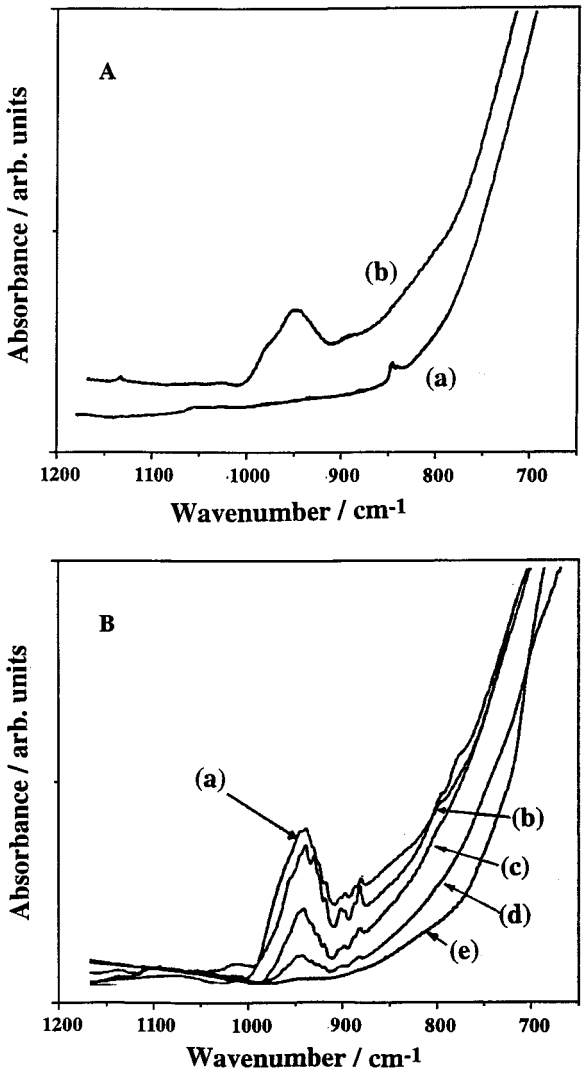

Figure 3. (A) Mid-infrared spectra of Cr(III)/SnO_2-cop (Cr:Sn 0.32) (a) dried at 333 K and (b) calcined at 573 K. (B) Mid-infrared spectra of Cr(III)/SnO_2-cop (Cr:Sn 0.32) after calcination at 573 K (a) and after further calcination at 673 (b), 873 (c), 1073 (d), and 1273 K (e).

$Me_3SnOSnMe_3$,[24] which occurs at 737 cm^{-1}. The weak broad band at ca. 470 cm^{-1} (not illustrated) is assigned to a symmetric Sn−O−Sn stretching mode.[23]

Figure 2 illustrates infrared spectra of Cr(VI)/SnO_2 (Cr:Sn 0.38) prior to and after calcination at various temperatures up to 1273 K. The bands at ca. 942 and 893 cm^{-1} in the spectrum of the uncalcined material are assigned to the Cr−O stretching modes of surface-adsorbed chromate(VI) species. These vibrations are assigned to the antisymmetric $\nu_{as}(CrO_3)$ and $\nu_{as}(CrO_4)$ vibrations of surface dichromate and chromate, respectively. The weak band at 903 cm^{-1} is the corresponding symmetric $\nu_s(CrO_3)$ vibration of the surface dichromate. These bands reduce in intensity with increased calcination due to reduction of chromium(VI) to chromium(III). Stretching modes of Cr(III)−O bonds appear at lower wavenumber than Cr(VI)−O modes and are masked by the broad Sn−O−Sn envelope.

Figure 3A illustrates the effects of calcination of

(23) Harrison, P. G.; Guest, A. *J. Chem. Soc., Faraday Trans. 1* **1987**, *83*, 3383.

(24) Kriegsman, H.; Hoffman, H.; Geissler, H. *Z. Anorg. Allg. Chem.* **1965**, *341*, 24.

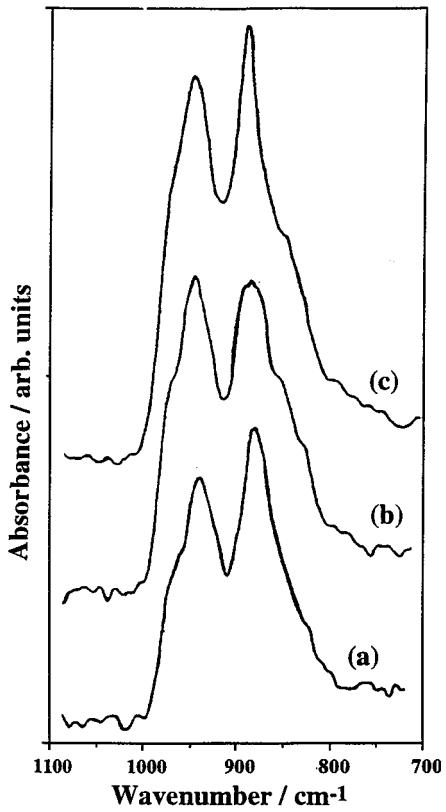

Figure 4. FT-Raman spectra for Cr(VI)/SnO_2-imp at Cr:Sn ratios of 0.12 (a), 0.23 (b), and 0.38 (c).

Cr(III)/SnO_2-cop (Cr:Sn 0.32) prior to and after calcination at 573 K, while Figure 3B shows the effect of further heating at various temperatures up to 1273 K. Although the spectrum of the material dried at 333 K is blank in the 850−1300 cm^{-1} region, a band at 948 cm^{-1} characteristic of the $\nu_{as}(CrO_3)$ vibration of surface dichromate is observed after calcination at 573 K (Figure 3A), which reduces in intensity with increased calcination temperature (Figure 3B). In addition, a much weaker band at 883 cm^{-1} characteristic of the $\nu_{as}(CrO_4)$ vibration of surface chromate is also observed. Thus, it appears that chromium(VI) species, predominantly dichromate together with small amounts of chromate, are formed at relatively low temperatures in the catalyst material derived from a chromium(III) precursor. As with the Cr(VI)/SnO_2 materials, these chromium(VI) species are destroyed on further heating but are not completely removed until 1273 K.

FT-Raman Spectroscopy Studies. Raman spectra in the range 750−1050 cm^{-1} (ν(Cr(VI)−O) region) for three uncalcined Cr(VI)/SnO_2-imp catalysts (Cr:Sn 0.12, 0.23, and 0.38) are illustrated in Figure 4 with assignments in Table 3. All three spectra are similar in form, exhibiting two principal maxima together with several shoulder features. The positions, however, of these maxima shift with different Cr:Sn ratios.

For the lowest loading (Cr:Sn 0.12), two broad weak bands are observed at ca. 886 and 946 cm^{-1}. The former band corresponds to the presence of surface-adsorbed CrO_4^{2-} anions while the latter indicates the presence of adsorbed $Cr_2O_7^{2-}$ anions (Table 3). The shoulder features at higher wavenumber indicate that species such as the $Cr_3O_{10}^{2-}$ anion are present in small amounts. It is also possible that higher species such as the $Cr_4O_{13}^{2-}$ anion are present.

Table 3. Assignment of FT-Raman Bands for Chromate Anions (cm^{-1})[a]

CrO_4^{2-}	$Cr_2O_7^{2-}$	$Cr_3O_{10}^{2-}$	$Cr_4O_{13}^{2-}$	assignment
		987	987	$\nu_{as}(CrO_2)$
		956	963	$\nu_s(CrO_2)$
	942			$\nu_{as}(CrO_3)$
886				$\nu_{as}(CrO_4)$
	904	904	902	$\nu_s(CrO_3)$
848				$\nu_s(CrO_4)$
		844	842	$\nu_{as}(Cr'OCr'')$

[a] From refs 25−28.

With increasing chromium loading, the peak maxima shift to 890/901 and 952 cm^{-1} and 901 and 959 cm^{-1} for Cr:Sn ratios 0.23 and 0.38, respectively. In all cases, pronounced shoulder features are present both at higher and lower wavenumber. This shift to higher wavenumber is explained by an increased concentration of adsorbed $Cr_2O_7^{2-}$ and $Cr_3O_{10}^{2-}$ anions. Studies by Michel and Cahay[29] have demonstrated that acidification of aqueous solutions of chromic acid (in this case higher concentration) results in a series of labile equilibria with a dominance of polyatomic chromate species. Thus, this increased concentration of adsorbed $Cr_2O_7^{2-}$ and $Cr_3O_{10}^{2-}$ species on the tin(IV) oxide surface is not unexpected. Adsorbed CrO_4^{2-} ions are also present, but only in small amounts. Broad bands due to SnO_2 appear at ca. 556 cm^{-1}, although the intensity of these bands decreases with increasing chromium(VI) concentration, indicating the increased coverage of the SnO_2 surface by adsorbed chromate ions.

It was not possible to obtain Raman spectra for the calcined catalyst materials.

X-ray Diffraction. Prior to calcination, all three types of materials exhibit diffractograms comprising four very broad peaks due to very small particulate SnO_2. No peaks are observed because of the chromium constituents, indicating an amorphous nature. A progressive increase in peak intensity coupled with a sharpening of the peaks is observed for all materials after calcination, indicating an increase in crystallinity of the SnO_2 phase. After calcination at 1273 K, all diffractograms are dominated by the characteristic pattern of tetragonal tin(IV) oxide.

The corundum Cr_2O_3 phase is identifiable for both chromium(VI)- and chromium(III)-promoted catalyst materials after calcination at 1273 K (parts d and c of Figure 5, respectively), with the most intense peaks at d (Å) values of {012} (3.631), {104} (2.665), {110} (2.480), {113} (2.175), {024} (1.815), and {116} (1.672).[30] The intensities of these peaks are small in comparison to the tin(IV) oxide pattern and also vary depending on the concentration of chromium present in the material; the higher the concentration, the greater the peak intensity. Some of the Cr_2O_3 peaks are masked by the intense tin(IV) oxide pattern; nevertheless, their presence can be elucidated by careful inspection as well as

(25) Vuurman, M. A. Ph.D. Thesis, University of Amsterdam, 1992.
(26) Hardcastle, F. D.; Wachs, I. E. *J. Mol. Catal.* **1989**, *46*, 173.
(27) Scharf, U.; Schneider, H.; Baiker, A.; Wokaun, A. *J. Catal.* **1994**, *145*, 464.
(28) Michel, G.; Cahay, R. *J. Raman Spectrosc.* **1986**, *17*, 4.
(29) Michel, G.; Cahay, R. *J. Raman Spectrosc.* **1986**, *17*, 79.
(30) JCPDS Pattern No. 21-1250 (SnO_2); JCPDS Pattern No. 38-1479 (Cr_2O_3).

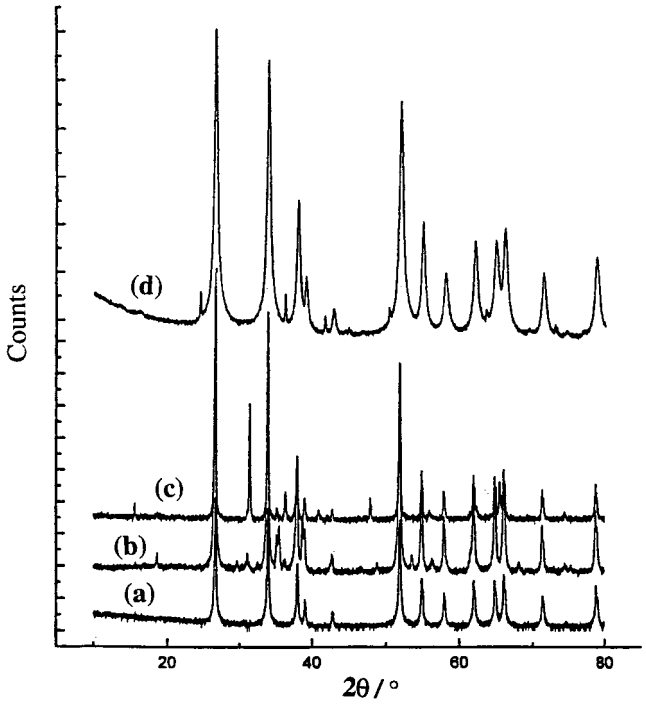

Figure 5. Powder X-ray diffraction pattern of (a) Cr(VI)/SnO_2-imp (Cr:Sn 0.38) calcined at 1273 K, Cr(III)/SnO_2-cop (Cr:Sn 0.32) calcined at 1073 (b) and 1273 K (c), and tin(IV) oxide (d).

Rietveld analysis (Figure 6). Cr(III)/SnO_2-cop materials exhibit patterns where the Cr_2O_3 peaks are considerably more intense than those for the Cr(VI)/SnO_2-imp materials where the preparative route is by impregnation. This is also reflected in the powder patterns after calcination at 873 and 1073 K where no peaks due to Cr_2O_3 are observable for Cr(VI)/SnO_2-imp, whereas Bragg reflections are observable for Cr_2O_3 after calcination at 873 K for Cr(III)/SnO_2-cop.

Investigations into the possibility of solid solution behavior, where chromium becomes incorporated in the rutile lattice, were made by indexing (DICVOL91) and Rietveld refinement. Results are given in Table 4 with representative Rietveld outputs for Cr(VI)/SnO_2-imp (Cr:Sn 0.38) and Cr(III)/SnO_2-cop (Cr:Sn 0.32) shown in Figure 6. Discrepancies between calculated and observed diffractograms can be rationalized by preferred orientation of crystallites. The indexed value for Cr(VI)/SnO_2-imp (Cr:Sn 0.38) possesses a high figure of merit and is within experimental error of the literature values,[30] thus indicating no thermally induced lattice incorporation of chromium. Therefore, it may be concluded that the promoting chromium exists solely as phase-separated Cr_2O_3 at elevated calcination temperatures and by implication no lattice incorporation of chromium occurs at lower calcination temperatures. For Cr(III)/SnO_2-cop (Cr:Sn 0.32) discrepancies between the indexed values (DICVOL91) and the literature values are evident. However, errors such as sample height could induce slight peak shifting (zero point error), resulting in a change in the observed lattice parameters. Zero-point error is accounted for in a Rietveld refinement, and lattice parameters derived in this way for Cr(III)/SnO_2-cop (Cr:Sn 0.32) are in accordance with the literature values,[30] therefore suggesting that no lattice incorporation is induced by thermal treatment for these materials also.

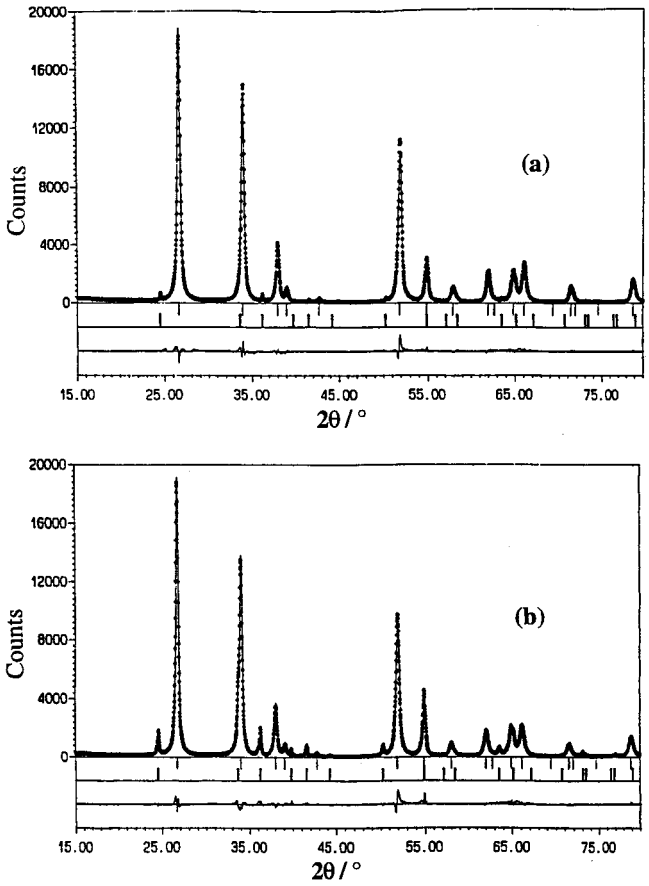

Figure 6. Rietveld refinement plots for (a) Cr(VI)/SnO_2-imp (Cr:Sn 0.38) calcined at 1273 K and (b) Cr(III)/SnO_2-cop (Cr:Sn 0.32) calcined at 1273 K. The upper tickmarks are for the SnO_2 phase, with the lower tickmarks indicating Cr_2O_3 peak positions. The correlation between the data points and the theoretically iterated pattern (solid line) is shown by the difference plot (lower trace).

Table 4. Lattice Parameters for SnO_2[a] Determined by Indexing and Rietveld Refinement

catalyst	DICVOL91 parameters/Å	figure of merit M(13)	Rietveld parameters/Å	R_{wp}
Cr(VI)/SnO_2-imp	$a = 4.736(3)$	177	$a = 4.734$	9.83
(Cr:Sn 0.38)	$c = 3.185(3)$		$c = 3.183$	
Cr(III)/SnO_2-cop	$a = 4.731(0)$	87	$a = 4.735$	9.67
(Cr:Sn 0.32)	$c = 3.179(1)$		$c = 3.183$	

[a] Reference values for tin(IV) oxide[30] are $a = 4.739$ Å and $c = 3.186$ Å.

Table 5. Values of Mean Crystallite Size Determined from X-ray Line Broadening for Cr(VI)/SnO_2-imp and Cr(III)/SnO_2-cop Materials

	mean particle size/nm					
catalyst	333 K	573 K	673 K	873 K	1073 K	1273 K
Cr(VI)/SnO_2-imp						
Cr:Sn 0.12	2.0	3.4	4.8	9.8	23.5	54.1
Cr:Sn 0.23	2.1	3.2	4.0	8.0	11.0	51.3
Cr:Sn 0.38	1.9	2.6	3.3	8.0	13.6	62.2
Cr(III)/SnO_2-cop						
Cr:Sn 0.12	1.3	1.8	2.5	3.8	11.6	29.3
Cr:Sn 0.32	1.4	1.5	1.8	2.6	11.0	35.1

Table 5 details the particle sizes calculated using the Scherrer equation values for various loadings of Cr(III)/SnO_2-cop and Cr(VI)/SnO_2-imp materials over a range of calcination temperatures. It is interesting to note that

the values obtained for Cr(III)/SnO_2-cop materials are generally lower than those for Cr(VI)/SnO_2-imp materials at the same calcination temperature. It would appear that coprecipitated materials exist as smaller primary crystallites which are more resilient to thermal sintering. A large increase in crystallite size for both material types is exhibited after calcination at temperatures ≥1073 K. Particles of both material types increase by ca. 30 times after calcination at 1273 K, although the coprecipitated materials are ca. 42% smaller than that of impregnated materials.

It should be stressed, however, that great caution must be taken with such calculated data because, in the preparation of the specimen for XRD analysis, the material is subjected to prolonged grinding to a fine powder in order to produce a densely packed slide for analysis. This grinding process subjects the material to excessive mechanical stress, and the local energy could quite possibly cause a sintering effect, producing larger particles for the XRD analysis. The opposite effect is the case for calcined materials where the mechanical force causes the large sintered particles to fracture, giving misleading size values in the XRD calculations. More accurate values can be obtained from TEM measurements. However, there are also various criteria associated with the preparation of TEM samples which can also affect mean particle size determinations.

TEM Studies. Parts a−f of Figure 7 are representative micrographs of Cr(VI)/SnO_2-imp (Cr:Sn 0.12) for the material dried at 333 K and after calcination at 573, 673, 873, 1073, and 1273 K, respectively. Parts g and h of Figure 7 are micrographs of Cr(III)/SnO_2-cop (Cr:Sn 0.32) after calcination at 1073 and 1273 K, respectively. Average particle sizes determined from a large number of micrographs are shown in Table 6 and corroborate the same trends as those determined from X-ray line broadening (Table 5).

The Cr(VI)/SnO_2-imp (Cr:Sn 0.12) material appears to be amorphous in character with an agglomeration of particles ranging in dimension from 2 nm for the material dried at 333 K up to 7 nm after calcination at 873 K (Figure 7a−d). A large increase in particle size is observed after calcination at ≥1073 K, with the particles having the appearance of rounded hexagons (Figure 7e,f), with lattice fringes indicating a high degree of crystallinity.

Similarly, the Cr(III)/SnO_2-cop (Cr:Sn 0.32) material appears to be amorphous in nature comprising aggregated particles ranging from 1.5 nm for the material dried at 333 K to regular shaped and sized particles up to 7 nm after calcination at 873 K. After calcination at 1073 K (Figure 7g) the particles are of a similar appearance but show a wide variation in size (10−20 nm). Lattice fringes are observable over large areas. After calcination at 1273 K (Figure 7h), the particles display a greater variation in size (20−60 nm) with extensive lattice fringing visible on most images extending over several particles, again indicating a high degree of crystallinity. EDXA analysis showed that the Sn and Cr compositions were in agreement with elemental analytical data and remained uniform for both the Cr(VI)/SnO_2-imp (Cr:Sn 0.12) and Cr(III)/SnO_2-cop (Cr:Sn 0.32) materials.

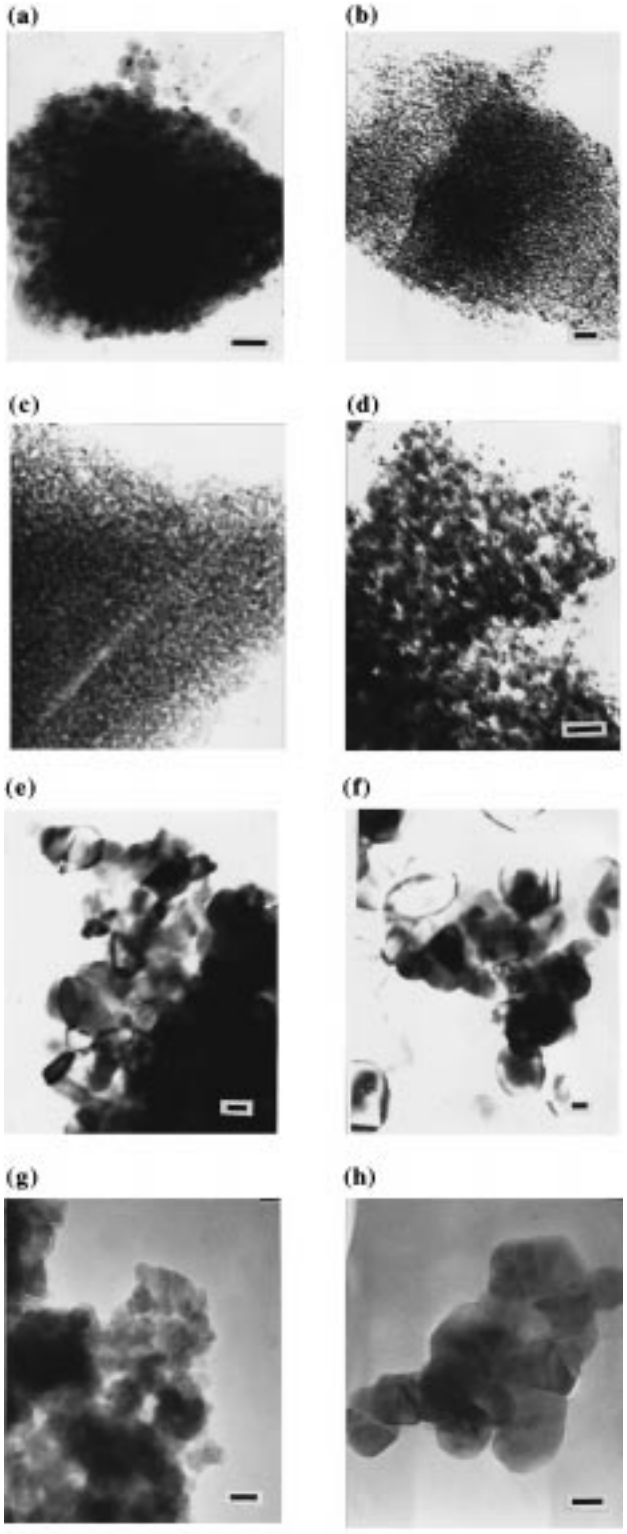

Figure 7. Transmission electron micrographs of Cr(VI)/SnO_2-imp (Cr:Sn 0.12) dried at 333 K (a) and after calcination at (b) 573, (c) 673, (d) 873, (e) 1073, and (f) 1273 K. g and h show micrographs of Cr(III)/SnO_2-cop (Cr:Sn:0.32) after calcination at 1073 and 1273 K, respectively.

Overall, good agreement is found between mean particle sizes determined by TEM and those calculated from XRD line broadening up to calcination temperatures of 873 K. A large increase in particle size is observed after calcination at 1073 K, and at 1273 K the particles are ca. 30−40 times greater than those for the

Table 6. Mean Particle Sizes for Cr(VI)/SnO_2-imp and Cr(III)/SnO_2-cop Materials Determined from TEM Micrographs

	mean particle size/nm					
catalyst	333 K	573 K	673 K	873 K	1073 K	1273 K
Cr(VI)/SnO_2-imp (Cr:Sn 0.12)	2 ± 0.5	2 ± 0.5	4 ± 1	7 ± 2	30 ± 5	56 ± 10
Cr(III)/SnO_2-cop (Cr:Sn 0.32)	1 ± 0.5	1 ± 0.5	2 ± 2	5 ± 2	15 ± 5	40 ± 20

[a] ± indicate size ranges.

uncalcined materials. The trend observed in XRD is seen also with TEM in that coprecipitated materials exhibit a greater resilience to thermal sintering than impregnated materials at elevated calcination temperatures. After calcination at 1273 K the particle size of coprecipitated materials are ca. 28% smaller than those for the impregnated materials. However, there are discrepancies between the values calculated from XRD patterns and those observed in TEM, as the particle sizes appear to be generally larger in the TEM. The major problem lies in the sample preparation stage of the analysis techniques. In the preparation of the microscope grid for TEM analysis, the material is subjected to sonification only. This would be expected to break interparticulate attractions only. However, as mentioned in the previous section, grinding powder samples for XRD analysis are very likely to fracture the larger particles induced by elevated calcination, thus resulting in misleading values.

XANES and EXAFS Studies. Chromium K-edge EXAFS spectra for Cr(VI)/SnO_2-imp (Cr:Sn 0.12) dried at 333 K and after calcination at calcination temperatures 573, 673, 873, 1073, and 1273 K are presented in Figure 8. The material dried at 333 K exhibits a prominent intense preedge peak at −4.3 eV, which decreases in intensity with increasing calcination temperature. For the Cr^{6+} ion, multiple-scattered-wave calculations have indicated that the preedge peak is due to an electronic transition from the Cr 1s orbital to an empty antibonding molecular orbital of primarily Cr 3d character.[31,32] This quadrupole, 1s → 3d, transition is "dipole-allowed" in a tetrahedral ligand field because of the extensive mixing of odd-parity Cr $3d_{z^2}$ and $4p_z$ orbitals with oxygen 2s and $2p_z$ orbitals. The intensity of the 1s → 3d transition varies with the number of d orbital vacancies, the site symmetry of the X-ray absorbing atom, and the metal−ligand bond length.[33] The immediate conclusion which may be made from this observation is that the oxidation state of chromium is +VI and is coordinated tetrahedrally (by oxygen) surrounded by a tetrahedral field of oxygen atoms.[34,35] This feature has previously[36] been observed in the XANES region for $Na_2CrO_4 \cdot 4H_2O$, $Na_2Cr_2O_7 \cdot 2H_2O$, and CrO_3, which exhibit an intense preedge peak at −4.1 to −4.3 eV, but not for chromium(III) compounds such as $Cr_2(SO_4)_3 \cdot 12H_2O$ and $CrK(SO_4)_2 \cdot 12H_2O$.

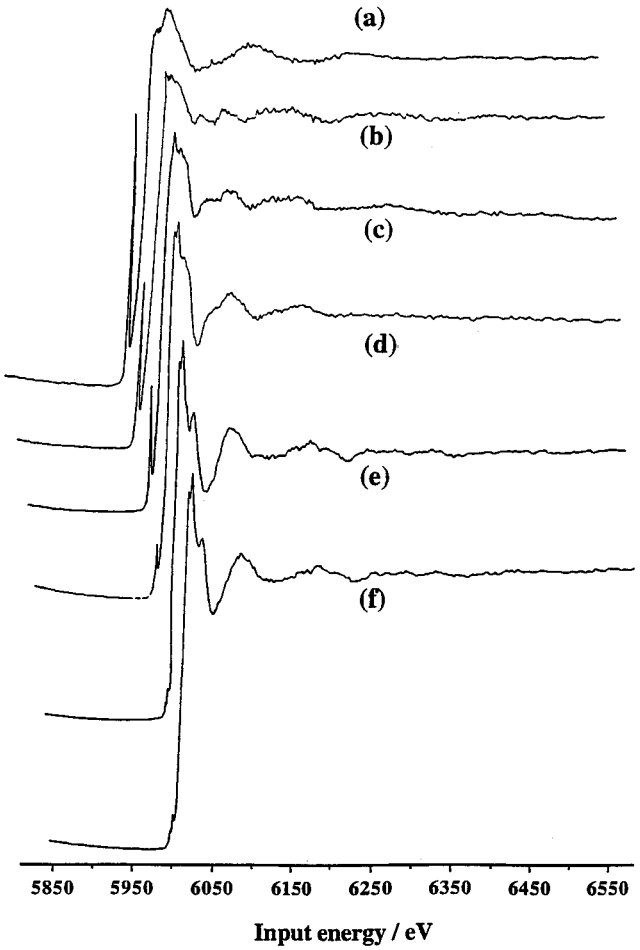

Figure 8. Cr K-edge EXAFS spectra for Cr(VI)/SnO_2-imp (Cr:Sn 0.12) after calcination at (a) 333, (b) 573, (c) 673, (d), 873, (e) 1073, and (f) 1273 K.

Table 7. Refined[a] Structural Parameters from Cr K-Edge EXAFS Data for Cr(VI)/SnO_2-imp

calcination temp	atom type	coord no.	Debye−Waller factor $2\sigma^2$/Å^2	radial distance/Å	chromium species present	lit. value/Å
333 K	O	4	0.010	1.649	$\{Cr_2O_7\}^{2-}$ [b]	1.663
	Cr	1	0.009	3.287		3.160
573 K	O	1	0.010	1.511	Cr_5O_{12}[c]	1.540
	O	2	0.040	1.631		1.642
	O	4	0.060	1.685		1.670
	O	1	0.004	1.707		1.805
	O	6	0.008	1.963		1.960
	Cr	1	0.005	2.990		3.060
	Cr	6	0.046	3.281		3.320
	Cr	1	0.008	3.828		3.824
	Cr	1	0.003	4.460		4.460
1273 K	O		0.010	1.900	Cr_2O_3[d]	1.960
	O	3	0.020	2.000		2.060
	Cr	1	0.015	2.647		2.700
	Cr	3	0.002	2.880		2.880
	Cr	3	0.012	3.390		3.470
	Cr	6	0.030	3.630		3.690

[a] *R* values 58.6 (333 K), 59.3 (573 K), and 52.0 (1273 K). [b] Reference 36. [c] Reference 37. [d] Reference 38.

Plots of normalized EXAFS data and their Fourier transforms for Cr(VI)/SnO_2-imp prior to calcination and after calcination at 573 and 1273 K are shown in Figure 9. The corresponding numerical data are collected in

(31) Kutzler, F. W.; Natoli, C. R.; Misemer, D. K.; Doniach, S.; Hodgson, K. O. *J. Chem. Phys.* **1980**, *73*, 327.
(32) Penner-Hahn, J. E.; Benfatto, M.; Hedman, B.; Takahashi, T.; Doniach, S.; Groves, J. T.; Hodgson, K. O. *Inorg. Chem.* **1986**, *25*, 2255.
(33) Wong, J.; Lytle, F. W.; Messmer, R. P.; Maylotte, D. H. *Phys. Rev. B* **1984**, *30*, 5596.
(34) Hawkins, J. K.; Isaacs, H. S.; Heald, S. M.; Tranquada, J.; Thompson, G. E.; Wood, G. C. *Corros. Sci.* **1987**, *27*, 391.
(35) Miyake, M.; Nakgawa, N.; Ohyanagi, H.; Suzuki, T. *Inorg. Chem.* **1986**, *25*, 700.
(36) Wainwright, J. S.; Murphy, O. J.; Antonio, M. R. *Corros. Sci.* **1992**, *33*, 281.

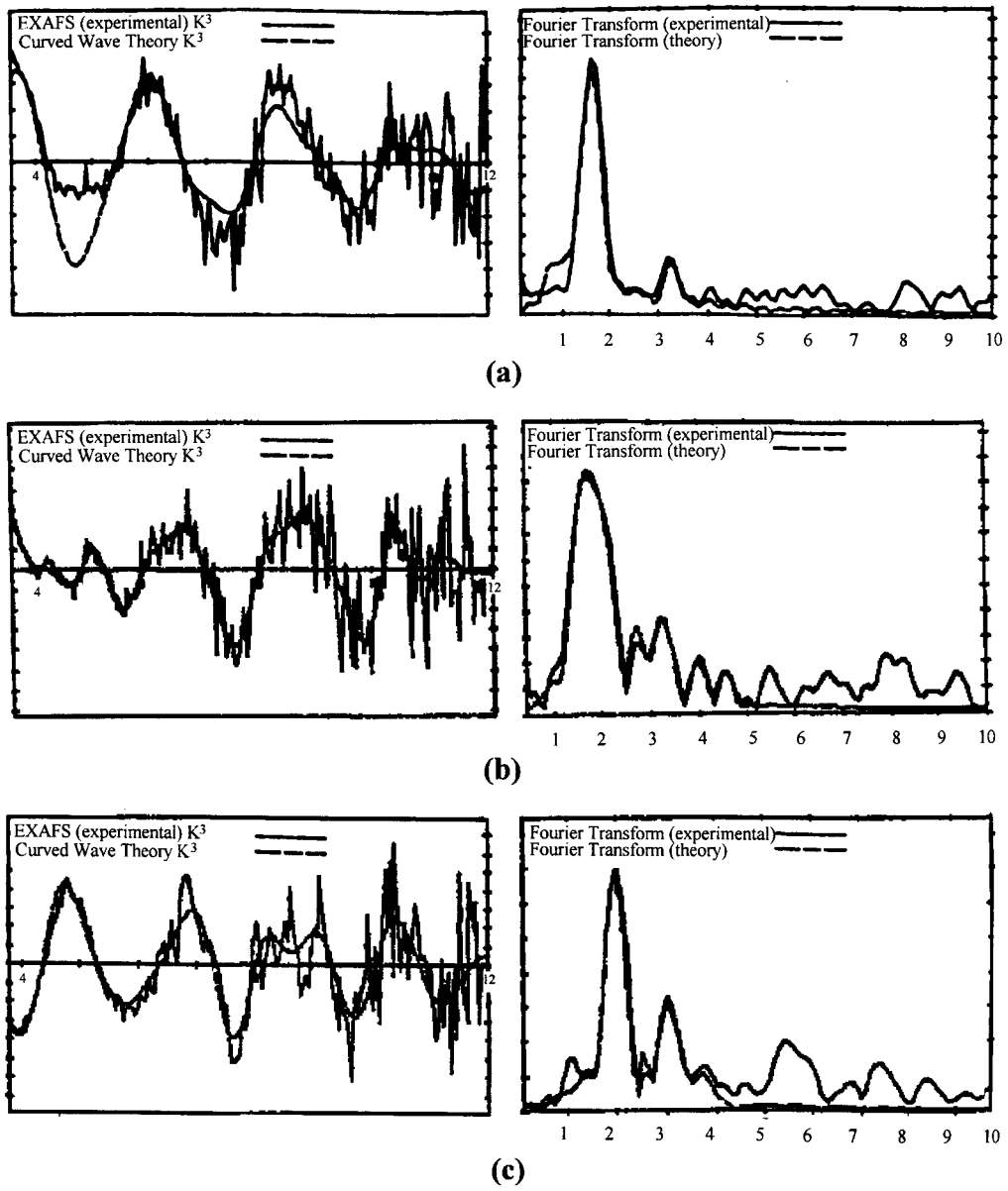

Figure 9. Experimental (solid line) and theoretical (dashed line) normalized EXAFS data and their Fourier transforms for Cr(VI)/SnO_2-imp (Cr:Sn 0.12) (a) dried at 333 K and calcined at 573 (b) and 1273 K (c).

Table 7. Coordination data for the Cr(VI)/SnO_2-imp (Cr:Sn 0.12) catalyst show that in the uncalcined material the chromium is four-coordinated by oxygen atoms at a mean distance of 1.649 Å with one chromium atom in the second coordination sphere at a distance of 3.287 Å. The Cr−O distance compares well with those determined by X-ray crystallography for $Na_2CrO_4 \cdot 4H_2O$[39] (1.645 Å), $Na_2Cr_2O_7 \cdot 2H_2O$[36] (1.663 Å), and CrO_3[40] (1.688 Å). The Cr−Cr distance of 3.287 Å is comparable with that in crystalline $Na_2Cr_2O_7 \cdot 2H_2O$[36] (3.160 Å). From this it can be concluded, in good agreement with the observations made with vibrational spectroscopy, that the chromium(VI) species present in this catalyst is principally the $[Cr_2O_7]^{2-}$ anion which is weakly bound, probably via hydrogen-bonding contacts, to the surface of the tin(IV) oxide particles. After calcination at 573 K, the mixed-valence oxide Cr_5O_{12} is produced, which has been described as a thermal decomposition product of CrO_3.[37] Discrepancies between the observed radial distances and those expected from the literature could arise from trace amounts of other chromium oxide phases. In the case of Cr(VI)/SnO_2-imp calcined at 573 K, this could be due to small amounts of CrO_3 crystallites remaining in the material. After calcination at 1273 K, the chromium-absorbing atoms exist as phase-separated Cr_2O_3, which are also observed in the powder XRD. Fits obtained from samples calcined between 573 and 1273 K correspond to amorphous Cr_2O_3, which becomes increasingly more crystalline with increasing calcination temperature.

Raw Cr K-edge data for both Cr(III)/SnO_2-imp (Cr:Sn 0.38) and coprecipitated Cr(III)/SnO_2-cop (Cr:Sn 0.32) are shown in Figures 10 and 11, respectively. It is interesting to note that both of these materials when calcined at 573 K exhibit preedge peaks a few electron-

(37) Wilmhelmi, K. A. *Acta Chem. Scand.* **1965**, *19*, 165.
(38) Newnham, R. E.; de Haan, Y. M. *Kurze Originalmitt.* **1962**, 235.
(39) Nimmo, J. K. *Acta Crystallogr., Sect. B* **1981**, *37*, 431.
(40) Stephens, J. S.; Cruickshank, D. W. J. *Acta Crystallogr., Sect. B* **1970**, *26*, 222.

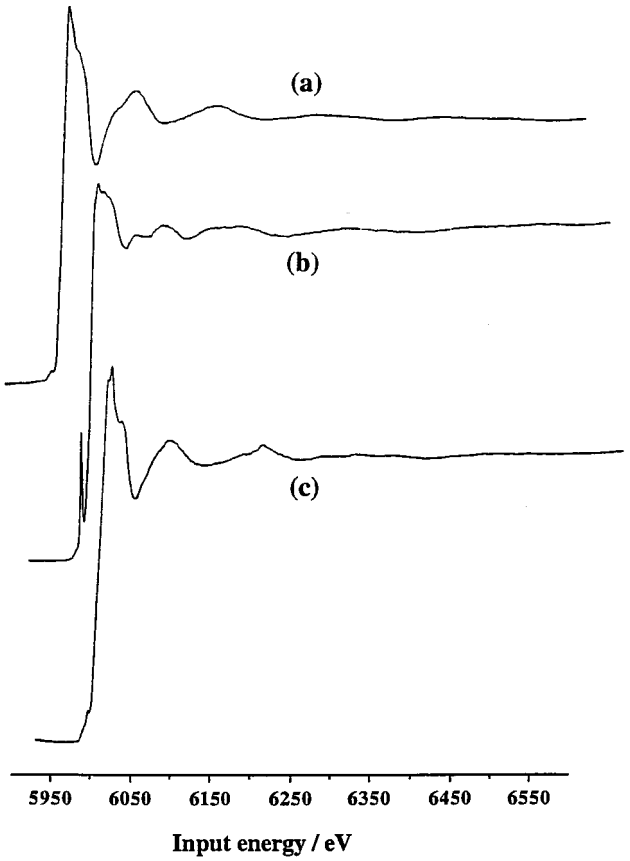

Figure 10. Cr K-edge EXAFS spectra for Cr(III)/SnO_2-imp (Cr:Sn 0.38) (a) dried at 333 K and calcined at 573 (b) and 1273 K (c).

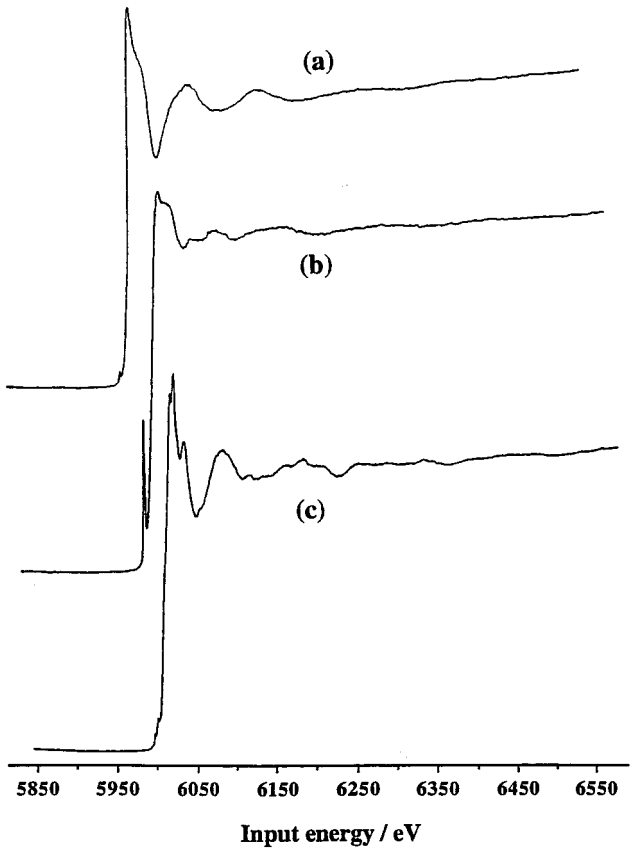

Figure 11. Cr K-edge EXAFS spectra for Cr(III)/SnO_2-cop (Cr:Sn 0.32) (a) dried at 333 K and calcined at 573 (b) and 1273 K (c).

volts below the Cr K-edge indicative of the presence of tetrahedrally coordinated chromium(VI) after this treatment as also shown by infrared. Results of data treatment are collected in Table 8 for Cr(III)/SnO_2-imp (Cr:Sn 0.38) and Table 9 for Cr(III)/SnO_2-cop (Cr:Sn 0.32). Plots of normalized EXAFS data and their Fourier transforms are shown in Figures 12 and 13, respectively.

A comparison of the data for Cr(III)/SnO_2-imp (Cr:Sn 0.38) and Cr(III)/SnO_2-cop (Cr:Sn 0.32) prior to calcination shows that different species are present in each. In the former, the chromium is present as hexaaqua $[Cr(H_2O)_6]^{3+}$ cations weakly bound, probably via hydrogen-bonding contacts, to the surface of the tin(IV) oxide particles. However, in the coprecipitated materials the chromium forms a γ-CrOOH local structure. In the first shell, six oxygen atoms are coordinated to the chromium at a distance of 1.985 Å. The second shell comprises two chromium atoms at 3.02 Å (edge-sharing CrO_6 octahedra) and a third shell of 1.5 chromium atoms at 3.98 Å (corner-sharing octahedra). The fit between the predicted and the experimental curves was greatly improved with the inclusion of a tin atom at 3.120 Å, affording some evidence for the anchoring of the complex to the surface of the oxide particle. These data are in good agreement with the structural parameters determined for γ-CrOOH.[42,43] Fendorf et al.[44] have observed similar behavior with Cr(III)/SiO_2 catalyst materials in which isolated hexaaqua $[Cr(H_2O)_6]^{3+}$ cations are present at low loadings of chromium, but γ-CrOOH is formed with increased chromium loading.

Table 8. Refined[a] Structural Parameters from Cr K-Edge EXAFS Data for Cr(III)/SnO_2-imp

calcination temp	atom type	coord no.	Debye–Waller factor $2\sigma^2$/Å^2	radial distance/Å	chromium species present	lit. value/Å
333 K	O	6	0.001	1.910	$Cr(H_2O)_6^{3+}$	
573 K	O	1	0.033	1.512	Cr_5O_{12}[b]	1.540
	O	2	0.003	1.613		1.642
	O	4	0.059	1.662		1.670
	O	1	0.002	1.757		1.805
	O	6	0.008	1.962		1.960
	Cr	1	0.005	3.000		3.060
	Cr	6	0.035	3.231		3.320
	Cr	1	0.001	3.846		3.824
	Cr	1	0.039	4.473		4.460
1273 K	O	3	0.001	1.930	Cr_2O_3[c]	1.960
	O	3	0.002	1.996		2.060
	Cr	1	0.001	2.661		2.700
	Cr	3	0.014	2.841		2.880
	Cr	3	0.009	3.410		3.470
	Cr	6	0.024	3.684		3.690

[a] *R* values 35.6 (333 K), 20.7 (573 K), and 36.2 (1273 K). [b] Reference 37. [c] Reference 38.

After calcination at 573 K, it appears that the Cr_5O_{12} oxide species is again produced in both Cr(III)/SnO_2-imp (Cr:Sn 0.32) and Cr(III)/SnO_2-cop (Cr:Sn 0.38). The determined structural parameters are again in good

(41) Fendorf, S. E.; Lamble, G. M.; Stapleton, M. G.; Kelley, M. J.; Sparks, D. L. *Environ. Sci. Technol.* **1994**, *28*, 284.
(42) Corker, J. M.; Evans, J.; Rummey, J. M. *Mater. Chem. Phys.* **1991**, *29*, 201.
(43) Fendorf, S. E.; Sparks, D. L. *Environ. Sci. Technol.* **1994**, *28*, 290.
(44) Eary, E. L.; Rai, D. *Environ. Sci. Technol.* **1987**, *21*, 547.

Table 9. Refined[a] Structural Parameters from Cr K-Edge EXAFS Data for Cr(III)/SnO_2-cop

calcination temp	atom type	coord no.	Debye–Waller factor $2\sigma^2$/Å^2	radial distance/Å	chromium species present	lit. value/Å
333 K	O	6	0.005	1.985	γ-CrOOH[b]	1.663
	Cr	2	0.019	3.020		3.160
	Sn	1	0.015	3.120		
	Cr	1.5	0.022	3.980		
573 K	O	1	0.018	1.503	Cr_5O_{12}[c]	1.540
	O	2	0.014	1.637		1.642
	O	4	0.018	1.652		1.670
	O	1	0.001	1.787		1.805
	O	6	0.012	1.949		1.960
	Cr	1	0.010	2.985		3.060
	Cr	6	0.046	3.243		3.320
	Cr	1	0.013	3.827		3.824
	Cr	1	0.009	4.454		4.460
1273 K	O	3	0.001	1.935	Cr_2O_3[d]	1.960
	O	3	0.002	1.997		2.060
	Cr	1	0.001	2.675		2.700
	Cr	3	0.014	2.861		2.880
	Cr	3	0.009	3.420		3.470
	Cr	6	0.024	3.676		3.690

[a] *R* values 24.0 (333 K), 37.0 (573 K), and 37.0 (1273 K). [b] Reference 41. [c] Reference 37. [d] Reference 38.

agreement with the literature values. The observed oxidation of Cr^{3+} to Cr^{6+} is unexpected, although the EXAFS provides strong evidence that this is clearly the case in this particular instance. Only manganese oxides are known to oxidize chromium(III) to chromium(VI), and the process is dependent upon the formation of a Cr(III)/MnO_2 complex.[44] EXAFS studies of the formation of chromia-pillared clay catalysts by Corker et al.[42,45] have also clearly demonstrated that chromium(III) precursors can be readily oxidized to Cr_5O_{12} under relatively mild calcination conditions (523–573 K). After calcination at 1273 K, the chromium-containing phase in both materials is Cr_2O_3 with the corundum structure.

Discussion

Three methods may be employed to prepare chromium-promoted tin(IV) oxide catalysts: (i) impregnation of SnO_2 using aqueous CrO_3 solutions, (ii) impregnation of SnO_2 using aqueous chromium(III) nitrate solutions, and (iii) coprecipitation from aqueous solutions containing both tin(IV) and chromium(III) ions. However, the nature of the freshly prepared gel materials is different in each case. All comprise small (ca. 1–2 nm) particles of hydrous tin(IV) oxide, on the surface of which are sorbed chromate(VI) anions (principally dichromate together with small amounts of monochromate and trichromate) (route i), $\{Cr(H_2O)_6^{3+}\}$ cations (route ii), or polymeric γ-CrO(OH) (route iii) depending on the preparative route. That different chromium(III) species are formed by routes ii and iii is not particularly surprising because the pH in route iii is significantly higher than that in route ii.

The loading of chromium in the two methods of catalyst preparation by impregnation (routes i and ii) can be controlled by careful control of the experimental variables affording a high degree of reproducibility. The elemental analytical data shown in Table 1 illustrate the sometimes quite dramatic disagreement between expected or "target" metal ratios and those actually present in the final catalyst when prepared by the coprecipitation route. As expected, prior to any thermal treatment the colors of the two series of catalyst derived using a chromium(III) source are green whereas the series of catalysts derived from a chromium(VI) source are yellow.

Optimum catalytic performance of chromium-promoted tin(IV) oxide materials is achieved after thermal activation in air in the temperature range 573–673 K.[8] After such treatment the catalytic activity is similar irrespective of whether the source of the chromium promoter is in oxidation state +III or +VI. Thermal treatment at more elevated temperatures results in a progressive lowering of activity for all materials. At this stage the appearance of the three types of catalysts is similar, all assuming a yellow or light brown color (cf. the characteristic green color of chromium(III)). The EXAFS spectra of both types of Cr(III)/SnO_2 catalysts exhibit a prominent preedge feature characteristic of tetrahedra chromium(VI). In addition, the infrared spectra of the Cr(III)/SnO_2-cop catalysts exhibit vibrations characteristic of chromate(VI) species. It is perhaps not surprising, therefore, that EXAFS studies demonstrate that the same chromium-containing species, the mixed-valence oxide Cr_5O_{12}, is present in all three types of catalyst materials after calcination at 573 K *irrespective of the origin of the chromium promoter*, whether it be adsorbed $\{Cr_2O_7\}^{2-}$ anions, adsorbed $\{Cr(H_2O)_6^{3+}\}$ cations, or adsorbed polymeric γ-CrO(OH). That the Cr_5O_{12} phase cannot be detected in the powder X-ray diffractograms indicates that it is amorphous in nature. Further, the uniformity of the unit cell data shows that no significant penetration of chromium into the rutile crystal lattice of the tin(IV) oxide occurs. We, therefore, propose that it is this composite oxide material comprising microparticulate Cr_5O_{12} dispersed on particulate tin(IV) oxide which is the active catalyst for hydrocarbon oxidation. At elevated temperatures crystalline α-Cr_2O_3 with the corundum structure is formed in all three cases consistent with the dark green appearance of the materials after calcination at 1273 K. These processes are summarized in Scheme 1.

Crystalline Cr_5O_{12} (average chromium oxidation state +4.8) is also formed in the thermal decomposition of CrO_3 under carefully controlled conditions (temperature range 513–533 K, oxygen pressures in the range of 2–3 kbar, 3–7 days).[37] This material is polymeric with a structure comprising pairs of edge-sharing $\{CrO_6\}$ octahedra linked to $\{CrO_4\}$ tetrahedra forming a three-dimensional network corroborating its nature as a mixed-valence oxide containing Cr(III) and Cr(VI), $Cr^{III}_2(Cr^{VI}O_4)_3$. It is notable that crystals of neat Cr_5O_{12} are black whereas the active catalysts described in the present case comprising amorphous Cr_5O_{12} supported on tin(IV) oxide are much paler, yellow or light brown, which strongly suggests some type of electronic interaction between the two components and would tend to support synergism in the operation of the catalytic activity.

Under ambient pressure the thermal decomposition of neat CrO_3 is reported to start at its melting point (470 K), but if heated above ca. 493 K, oxygen is lost stepwise

(45) Bornholt, K.; Corker, J. M.; Evans, J.; Rummey, J. M. *Inorg. Chem.* **1991**, *30*, 2.

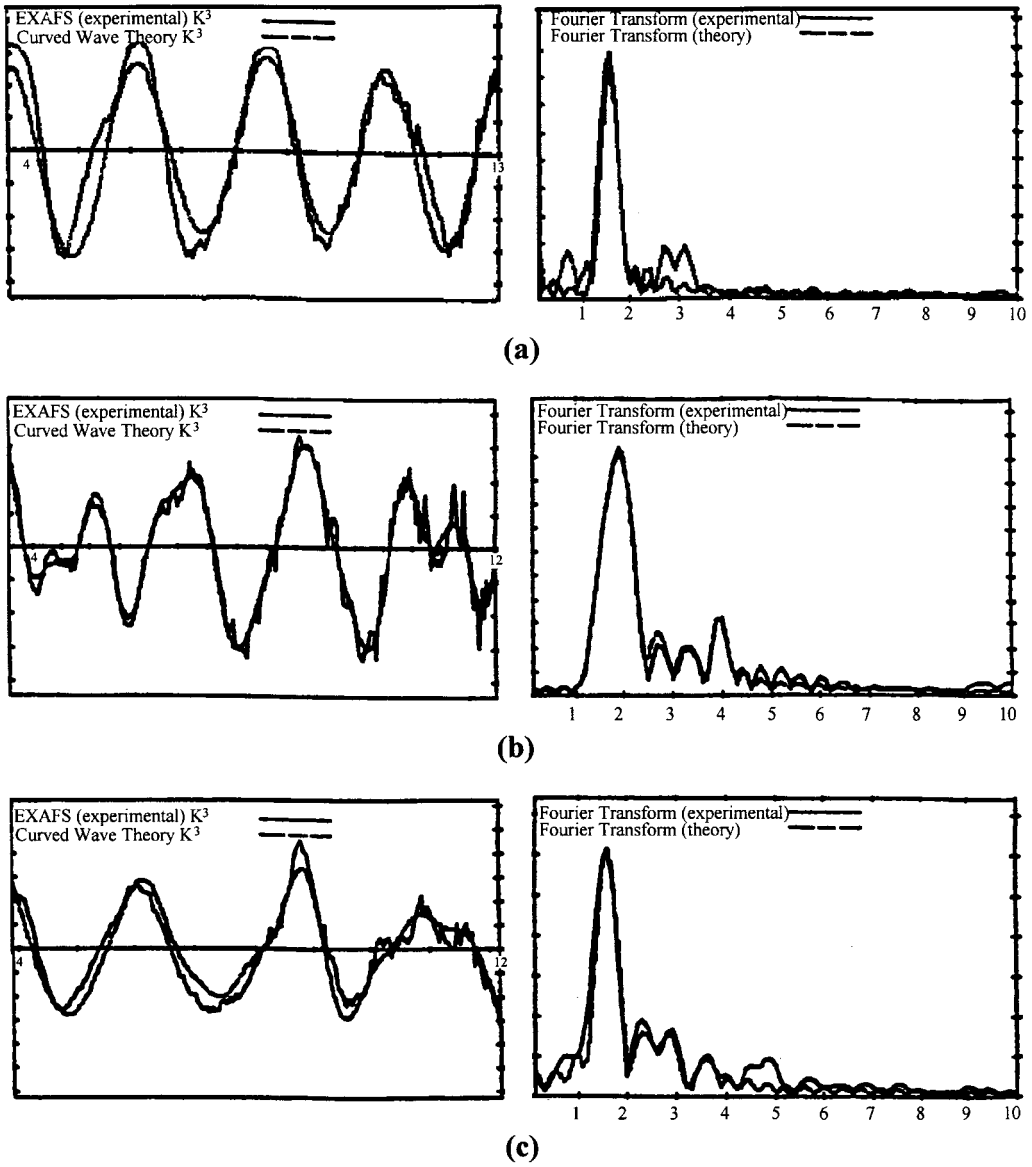

Figure 12. Experimental (solid line) and theoretical (dashed line) normalized EXAFS data and their Fourier transforms for impregnated Cr(III)/SnO_2-imp (Cr:Sn 0.38) (a) dried at 333 K and calcined at 573 (b) and 1273 K (c).

to form a succession of lower oxides including Cr_3O_8 (average chromium oxidation state +5.33), Cr_2O_5 (average chromium oxidation state +5), and CrO_2 (chromium oxidation state +4) until the eventual formation of α-Cr_2O_3 at ca. 720 K (Scheme 2).[46] Consistent with these findings, in a separate study Cr_2O_5 was shown to be formed from the decomposition of CrO_3 at 573 K, with α-Cr_2O_3 again being formed at higher temperatures (873 K).

In contrast, hydrous chromium(III) oxide prepared by precipitation from aqueous solution undergoes only dehydration albeit in several stages before eventually forming α-Cr_2O_3 (Scheme 3).[47,48] However, decomposition of chromium(III) nitrate hydrate, $Cr(NO_3)_3 \cdot 9H_2O$, at 573 K afforded poorly crystallized α-Cr_2O_3, with minority bulk and surface Cr^{4+} and Cr^{6+} species showing that some oxidation of the chromium(III) to higher oxidation states (presumably by nitrate) can occur. At higher temperatures well-crystallized α-Cr_2O_3 with surface chromates was formed.[49]

Thermal decomposition behavior of $Cr(NO_3)_3 \cdot 9H_2O$ and CrO_3 supported on silica and alumina behaves in a fashion broadly similar to that of the unsupported compounds.[49−51] Heating the Cr(III)/SiO_2 and Cr(VI)/SiO_2 materials at 573 K afforded poorly crystallized supported chromium oxides of stoichiometries $CrO_{2.1}$ and $CrO_{2.6}$, respectively, whereas at 873 K large crystallites of α-Cr_2O_3 are formed in both cases. The only effect of the silica support appears to be the formation of smaller chromium oxide particle sizes. No crystalline chromia species were formed on alumina as a support material irrespective of calcination temperature al-

(46) Kubota, B. *J. Am. Ceram. Soc.* **1961**, *44*, 239.

(47) Singh, K. K.; Sarade, P. R.; Ganguly, P. *J. Chem. Soc., Dalton Trans.* **1983**, 1895.

(48) Spiccia, L.; Marty, W.; Giovanoli, R. *Helv. Chim. Acta* **1987**, *70*, 1737.

(49) Fouad, N. E.; Knozinger, H.; Zaki, M. I. *Z. Phys. Chem.* **1994**, *186*, 231.

(50) Fouad, N. E.; Knozinger, H.; Ismail, H. M.; Zaki, M. I. *Z. Phys. Chem.* **1991**, *173*, 201.

(51) Fouad, N. E.; Knozinger, H.; Zaki, M. I.; Mansour, S. A. A. *Z. Phys. Chem.* **1991**, *181*, 75.

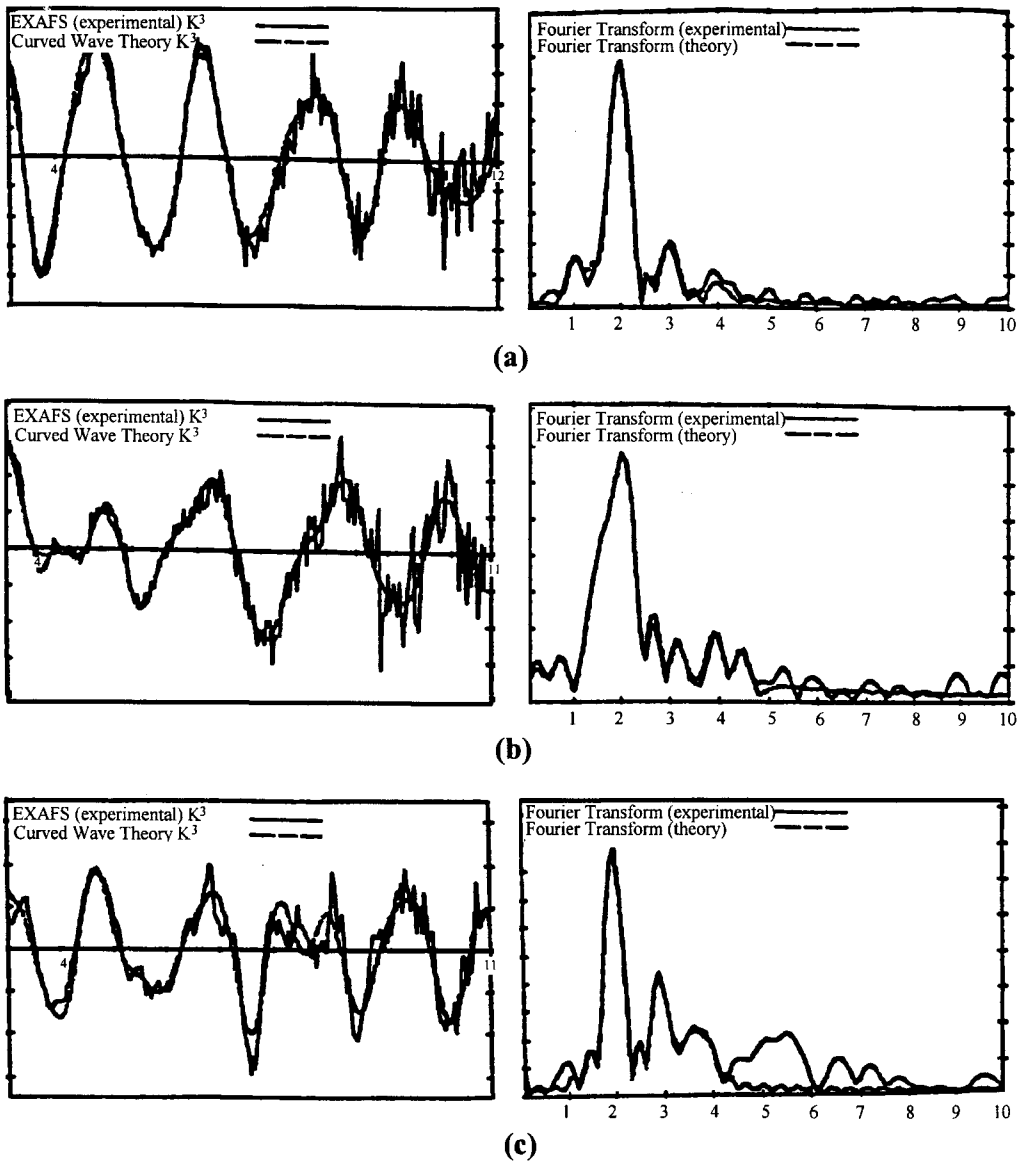

Figure 13. Experimental (solid line) and theoretical (dashed line) normalized EXAFS data and their Fourier transforms for coprecipitated Cr(III)/SnO_2-cop (Cr:Sn 0.32) (a) dried at 333 K and calcined at 573 (b) and 1273 K (c).

Scheme 1. Thermal Transformations of Chromium Species Supported on Tin(IV) Oxide

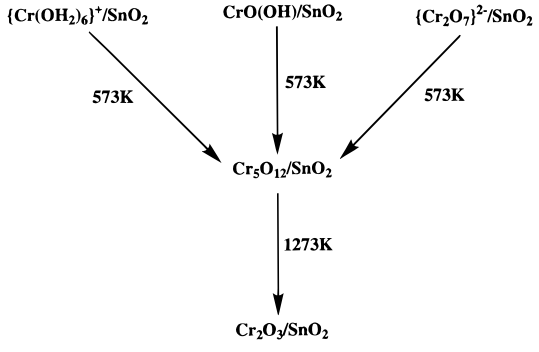

Scheme 2. Stages in the Thermal Transformation of CrO_3 to α-Cr_2O_3 (after Reference 46)

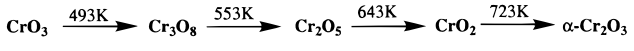

though very weak X-ray diffraction features of α-Cr_2O_3 are observed at 873 K. The stoichiometry of the chromium oxide species formed on alumina is independent

Scheme 3. Stages in the Thermal Transformation of $Cr(OH)_3 \cdot 3H_2O$ to α-Cr_2O_3 (after References 47 and 48)

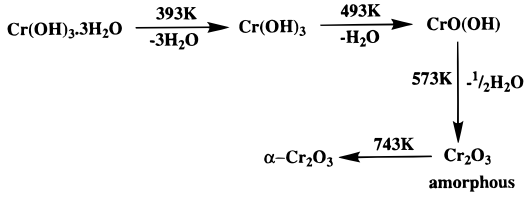

of the oxidation state of the chromium source and is determined only by the temperature of calcination, with a stoichiometry of $CrO_{2.2}$ being formed at 573 K and that of $CrO_{1.7-1.8}$ being formed at 873 K. It would appear, therefore, that the predominant species formed on alumina after calcination at 573 K is chromium(IV) oxide, CrO_2.

Compared to alumina or silica, tin(IV) oxide is a relatively oxidizing medium, and therefore it is not too surprising that sorbed chromium(III) species on tin(IV) oxide undergo transformation to higher oxidation states. What is perhaps surprising is the formation of the

discrete well-defined phase Cr_5O_{12} both from chromium +3 and +6 precursors supported on tin(IV) oxide after calcination at 573 K. At this temperature neat crystalline CrO_3 affords Cr_2O_5 whereas ill-defined chromium oxides of stoichiometry $CrO_{2.1-2.6}$ are formed when supported on silica or alumina, and chromium(III) nitrate gives Cr_2O_3 with small amounts of chromium +4 and +6 species both neat as well as when supported on silica and alumina after the same thermal treatment.

Conclusions

Three methods may be employed to prepare chromium-promoted tin(IV) oxide catalysts: (i) impregnation of SnO_2 using aqueous CrO_3 solutions, (ii) impregnation of SnO_2 using aqueous chromium(III) nitrate solutions, and (iii) coprecipitation from aqueous solutions containing both tin(IV) and chromium(III) ions. However, the nature of the freshly prepared gel materials is different in each case. All comprise small (ca. 1−2 nm) particles of hydrous tin(IV) oxide on the surface of which are sorbed chromate(VI) anions (route i), $\{Cr(H_2O)_6^{3+}\}$ cations (route ii), or polymeric γ-CrOOH (route iii) depending on the preparative route. Nevertheless, the same catalyst material appears to be formed in all cases irrespective of preparative route after calcination at 573 K, when the active catalyst comprises the mixed-valence chromium compound Cr_5O_{12} supported on tin(IV) oxide. At higher calcination temperatures Cr_2O_3 is formed, which becomes more crystalline the higher the temperature. Concurrently, the size of the tin(IV) oxide particles increases, only slowly initially (ca. ×2 by 673 K and ca. ×4 by 873 K), but sintering to very large particles occurs at higher temperatures. No incorporation of chromium into the tin(IV) oxide lattice occurs even after calcination at high temperatures.

Acknowledgment. We thank the Commission of the European Community (Contract No. AVI* CT92-0012) and the EPSRC (for Research Grant No. GR/J76026 and providing facilities at DRAL) for support and the Malaysian Government (for the award of a scholarship to W.A.).

CM980347P